Electronic Supplementary Information

A highly efficient metal-free electrocatalyst of nitrogen-doped porous carbon nanoflowers toward oxygen electroreduction

Xiaoli Fan,[a] Yingying Zhang,[a]* Qinghong Geng,[a] Longlong Fan,[a] Wei Zhu,[a] Esmail Doustkhah,[c] Cuiling Li[b]*

[a]School of Chemistry and Chemical Engineering, Beijing Institute of Technology, Beijing 100081, China

E-mail: zhangyingying@bit.edu.cn

[b]CAS Key Laboratory of Bio-inspired Materials and Interfacial Science, Technical Institute of Physics and Chemistry, Chinese Academy of Sciences, Beijing 100190, China

E-mail: licuiling@mail.ipc.ac.cn

[c]Chemistry Department, Faculty of Engineering and Natural Sciences, Istinye University, 34396 Sarıyer, Istanbul, Turkey

Experimental Procedures

Chemicals. Dopamine hydrochloride (98%, Sigma-Aldrich), polyvinyl pyrrolidone (PVP, Sigma-Aldrich), 2-methylimidazole (2-MeIM, 98%, Aladdin), zinc nitrate hexahydrate ($Zn(NO_3)_2 \cdot 6H_2O$, ≥ 99%, Xilong Scientific), ammonia solution ($NH_3 \cdot H_2O$, 25-28%, Shanghai Titan Scientific), methanol (99.5%, Shanghai Titan Scientific) and ethanol (99.7%, Shanghai Titan Scientific) were used without further purification. Deionized water is used in all experiments.

Characterization. A field emission scanning electron microscope (SEM, Zeiss Supra 55, Zeiss, Germany) operating at 20 kV was used to observe the morphology of PCNFs nanoparticles. Transmission electron microscopy (TEM), high-angle annular dark field (HAADF) images and energy-dispersive X-ray (EDX) mapping were observed with a FEI, Talos F200X apparatus (Thermo Fisher, the United States) at an accelerating voltage of 200 kV. Fourier transform infrared (FTIR) spectra were collected on a Bruker FTIR spectrophotometer in the range of 2700-900 cm^{-1} using KBr pellets. X-ray photoelectron spectroscopy (XPS) analysis was conducted on PHI 5000 Versaprobe III scanning microprobe multi-functional X-ray photoelectron spectroscopy (ULVAC-PHI, Japan). The binding energies of all the peaks were calibrated by using the adventitious C 1*s* peak (284.8 eV) as an internal standard. Meanwhile, all the obtained XPS spectra were further analyzed and deconvoluted by using the software of Thermo Avantage. Raman spectra were achieved by LabRAM HR Evolution (HORIBA, Japan) with an excitation laser wavelength of $\lambda = 514$ nm. The nitrogen adsorption-desorption isotherms of the samples were acquired by using a BELSORP-max analyzer (Ankersmid, Holland). X-ray diffraction (XRD) characterization was carried recorded on Ultima IV X-ray diffractometer (Rigaku, Japan) at a scanning rate of 2 degrees per min with a Cu-Ka radiation (40 kV, 40 mA) source.

Synthesis of ZIF-8-based nanoflowers. The ZIF-8-based nanoflowers were prepared by a polymer-assisted approach. In a typical synthesis, 30.0 mg of PVP and 80.0 mg of dopamine were first dissolved in 10.0 mL of mixed deionized water and methanol solution (volume ratio of 1:1), followed by the addition of 65.0 uL of $NH_3 \cdot H_2O$. Then, the mixture was stirred at 60.0 ℃ for 0.5 h. After that, 420.0 mg of 2-MeIM were added

to the solution, followed by the addition of 10.0 mL of mixed deionized water/methanol solution (volume ratio of 1:1), which consisted of 30.0 mg of PVP and 1480.0 mg of $Zn(NO_3)_2 \cdot 6H_2O$. After reacting for 2.0 h, the brown precursor was subjected to centrifugal filtration and washed with ethanol and water several times. The obtained brown precursors were then dried at 60.0 °C under vacuum to obtain the final ZIF-8-based nanoflowers.

In this work, various dosages of PVP (*e.g.*, 0, 20.0 or 40.0 mg) were used to study its effect on morphology of materials. Meanwhile, the effect of polydopamine (PDA) on the morphology was then evaluated by varying the dosages of dopamine (*e.g.*, 0, 20.0, 60.0 or 100.0 mg), while PVP dosages was 30.0 mg. In addition, in order to explore the effect of ZIF-8 nanosheets on morphology of the precursor, PDA nanosheets was also synthesized in the absence of raw materials for the synthesis of ZIF-8 nanosheets.

Synthesis of nitrogen-doped porous carbon nanoflowers (N-PCNFs). To prepare nitrogen-doped porous carbon nanoflowers (N-PCNFs) with different pyridinic-N content, the obtained ZIF-8-based nanoflowers by changing the dosage of PVP were transferred to a tube furnace and pyrolyzed at 1000.0 ℃ for 2.0 h under the protection of argon atmosphere. According to the amount of pyridinic-N, the catalysts derived from PVP dosages of 0, 20.0, 30.0 and 40.0 mg were denoted as N-PCNFs-9.6, N-PCNFs-13.3, N-PCNFs-43.5 and N-PCNFs-17.0, respectively.

To prepare nitrogen-doped porous carbon nanosheets (N-PCNSs), ZIF-8 nanosheets was pyrolyzed under the same condition of N-PCNFs.

Electrochemical measurements. The electrocatalytic measurements were performed in a three-electrode cell using a rotating disk electrode (RDE) with a CHI-760 electrochemical workstation. The platinum plate (1.0 cm ×1.0 cm) and Ag/AgCl electrode were used as the counter electrode (CE) and reference electrode (RE), respectively. An aqueous solution of 0.1 M KOH was used as electrolyte. Before running electrochemical tests, either gaseous N_2 or O_2 was purged into the electrolyte for 0.5 h to obtain N_2- or O_2-saturated electrolyte. The ink of catalysts was prepared by ultrasonically dispersing 5.0 mg catalyst in 1.0 mL mixture solvent of 950.0 μL of ethanol-water solution and 50.0 μL of 5 wt% Nafion solution. The ink was sonicated

for 1.0 h to get a homogeneous suspension. Then, 20.0 μL of the ink was dropped onto the glassy carbon electrode and dried at room temperature. The mass loading was 0.42 mg cm^{-2} for all the catalysts. The cyclic voltammetry (CV) tests were collected at a scan rate of 50.0 mV s^{-1} and the linear sweep voltammetry (LSV) polarization curves were conducted at a sweep rate of 10.0 mV s^{-1}. CV curves in the region of 1.0-1.1 V *vs.* RHE were measured in N_2-saturated 0.1 M KOH solution under different scan rates. All potentials in this study refer to the reversible hydrogen electrode (RHE), $E_{RHE} = E_{Ag/AgCl} + 0.197 + 0.0591 \times pH$. The number of electrons transferred (n) during ORR was calculated by Koutecky-Levich (K-L) equation[S2,S3]:

$$\frac{1}{J} = \frac{1}{J_L} + \frac{1}{J_K} = \frac{1}{B\omega^{\frac{1}{2}}} + \frac{1}{J_K}$$

$$B = 0.62nFC_{O_2}D_{O_2}^{\frac{2}{3}}V^{-\frac{1}{6}}$$

$$J_K = nFkC_{O_2}$$

where J, J_L and J_K are the measured current density, kinetic and diffusion limiting current densities, respectively, ω is the angular frequency of rotation ($\omega = 2\pi f/60$, f is the RDE rotation rate in rpm), n is the number of electrons transferred, F is the Faraday's constant (96485 C mol^{-1}), D_{O_2} is the diffusion coefficient of O_2 in 0.1 M KOH solution (1.9×10^{-5} cm^2 s^{-1}), C_{O_2} is the concentration of molecular oxygen in 0.1 M KOH solution (1.2×10^{-6} mol cm^{-3}), V is the kinematic viscosity of the electrolyte (0.01 cm^2 s^{-1}) and k is the electron-transfer rate constant.

The electron transfer number (n) were determined by the following equations:

$$n = 4 \times \frac{I_D}{I_D + \frac{I_R}{N}}$$

where, I_D is the disk current, I_R is the ring current, and $N = 0.4$ is the current collection efficiency of the Pt ring.

The electrochemically active surface area (ECSA) was determined by non-faradic double-layer capacitance and obtained by the following equation[S4,S5]:

$$\mathrm{ECSA} = \frac{C_{\mathrm{dl}}}{C_{\mathrm{s}}}$$

where C_{dl} is double layer capacitance, Cs (0.04 $mF \cdot cm^{-2}$) represents the specific capacitance of the total double layer.

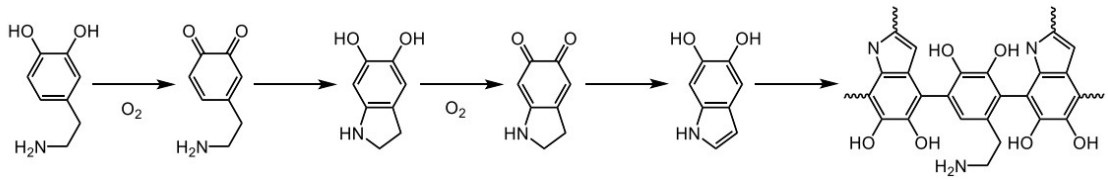

Fig. S1. The polymerization mechanism of dopamine for the formation of PDA.

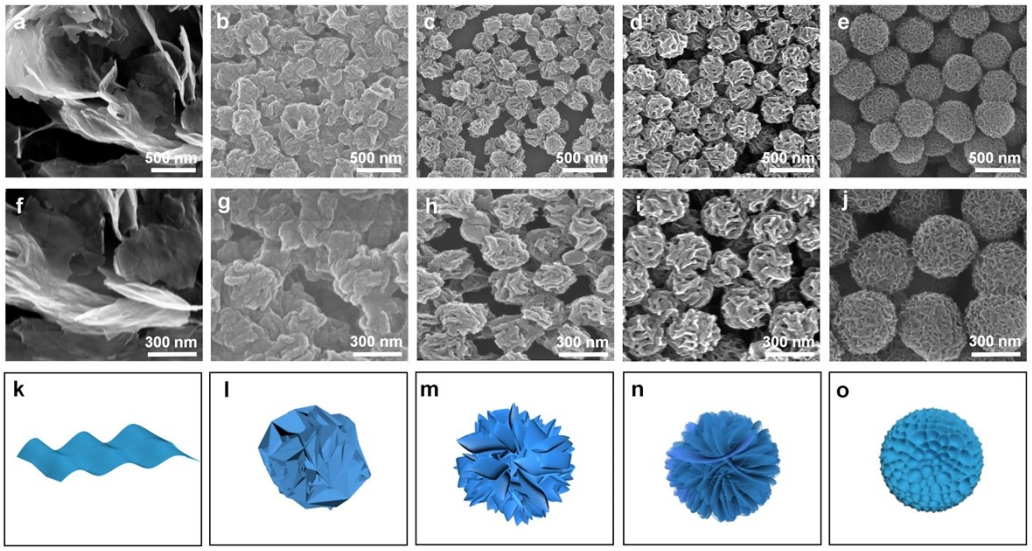

Fig. S2. (a-j) SEM images and (k-o) schematic images of products prepared with different dosages of dopamine: (a, f, k) 0 mg, (b, g, i) 20.0 mg, (c, h, m) 60.0 mg, (d, i, n) 80.0 mg and (e, j, o) 100.0 mg.

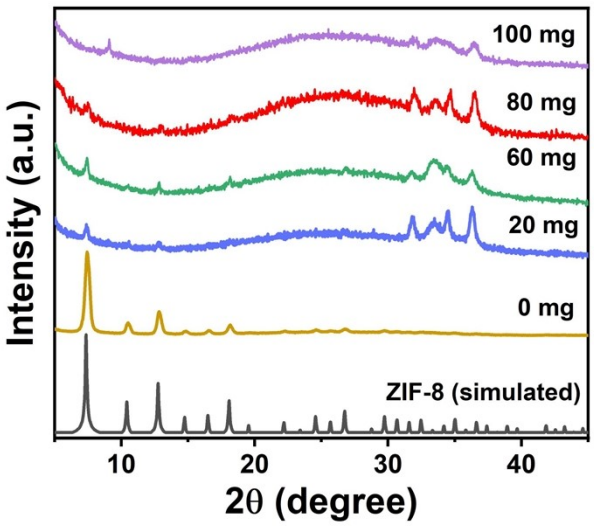

Fig. S3. XRD patterns of ZIF-8-based products prepared under the typical condition but using different dosages of dopamine.

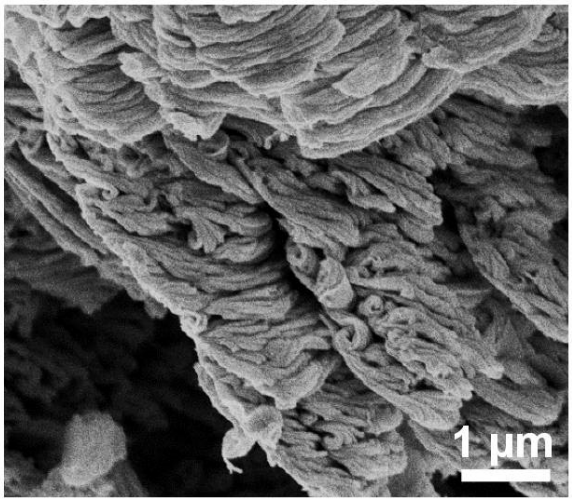

Fig. S4. SEM image of PDA synthesized under the typical condition but without adding 2-MeIM and $Zn(NO_3)_2$.

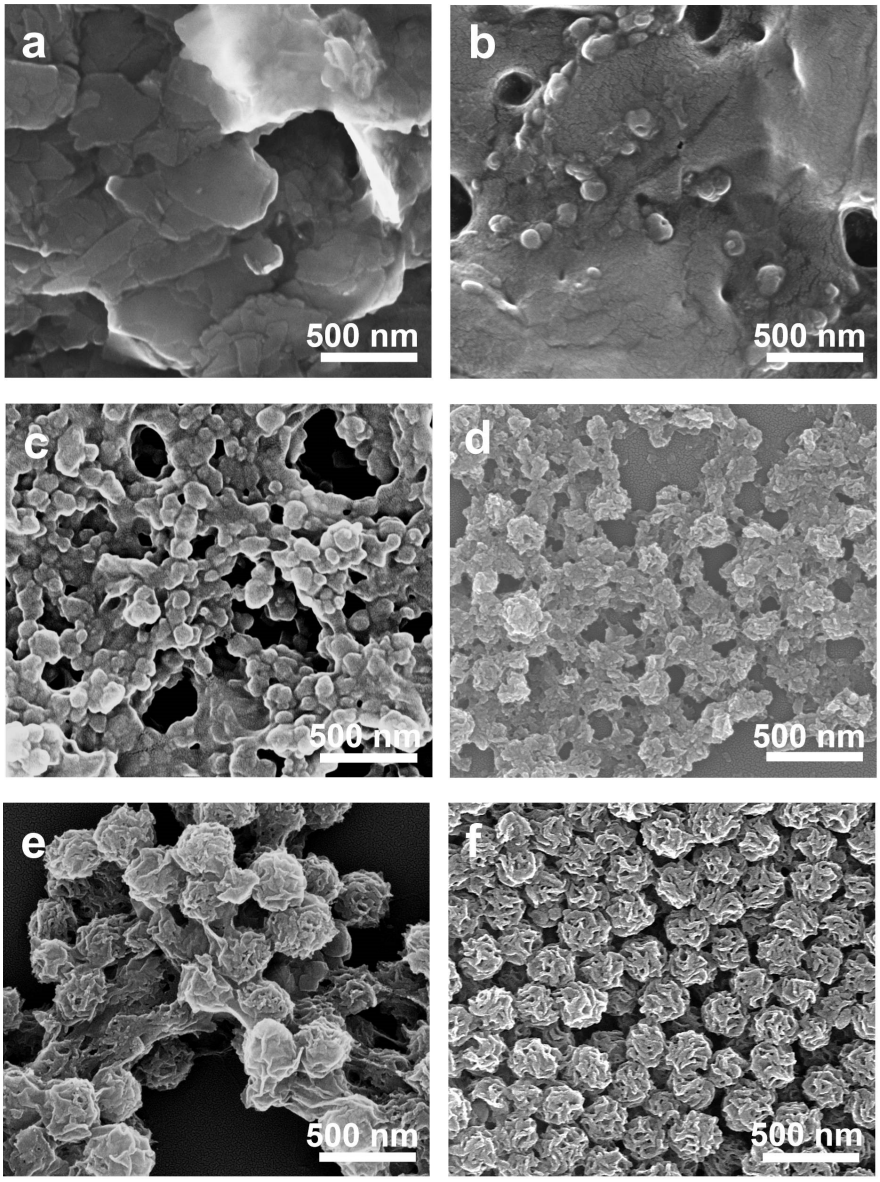

Fig. S5. SEM images of ZIF-8-based nanoflowers products prepared with different reaction time: (a) 30.0 min, (b) 35.0 min, (c) 45.0 min, (d) 60.0 min, (e) 90.0 min and (d) 120.0 min.

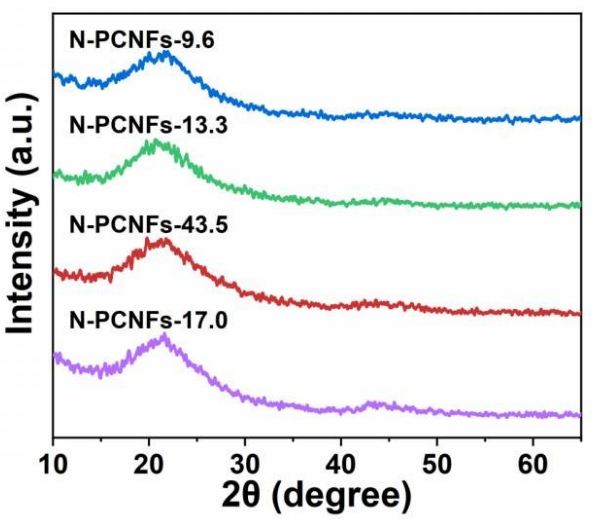

Fig. S6. XRD patterns of N-PCNFs samples.

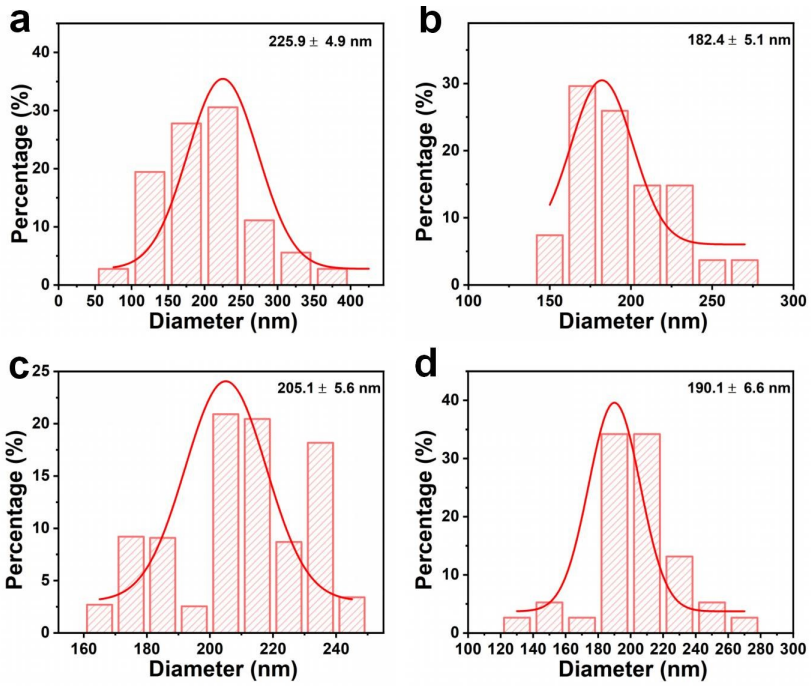

Fig. S7. Size distribution of (a) N-PCNFs-9.6, (b) N-PCNFs-13.3, (c) N-PCNFs-43.5 and (d) N-PCNFs-17.0.

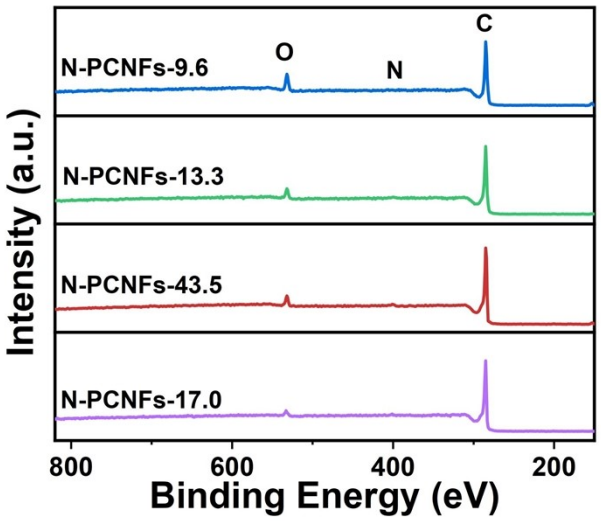

Fig. S8. The XPS survey spectra of N-PCNFs samples.

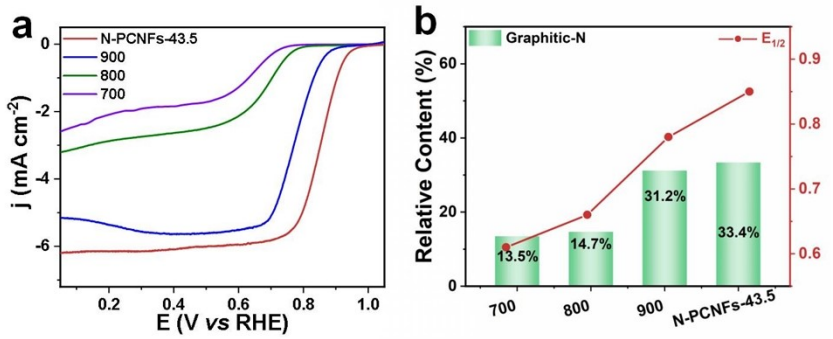

Fig. S9. (a) LSV curves of the investigated catalysts recorded in the O_2-saturated alkaline solution at 1600 rpm and 10 mV s^{-1}. (b) Comparison of half-wave potential and the content of graphitic-N in different samples.

Notes: The samples named by 700, 800, 900 and N-PCNFs-43.5 were derived from same ZIF-8-based precursor, and they were obtained N-doped porous carbon nanoflowers under pyrolyzed temperature of 700.0 ℃, 800.0 ℃, 900.0 ℃ and 1000.0 ℃, respectively.

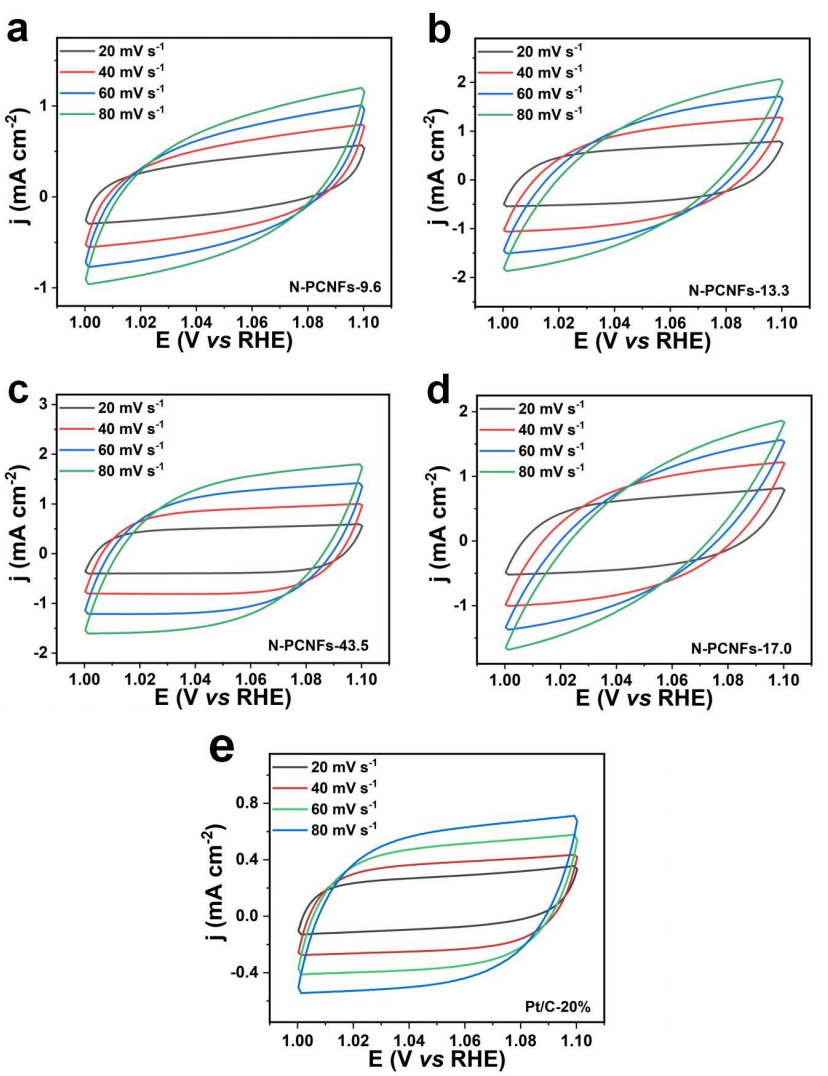

Fig. S10. CV curves at a potential range of 1.0 and 1.1 V at different scan rates for (a) N-PCNFs-9.6, (b) N-PCNFs-13.3, (c) N-PCNFs-43.5 (d) N-PCNFs-17.0 and (e) commercial Pt/C-20% catalyst.

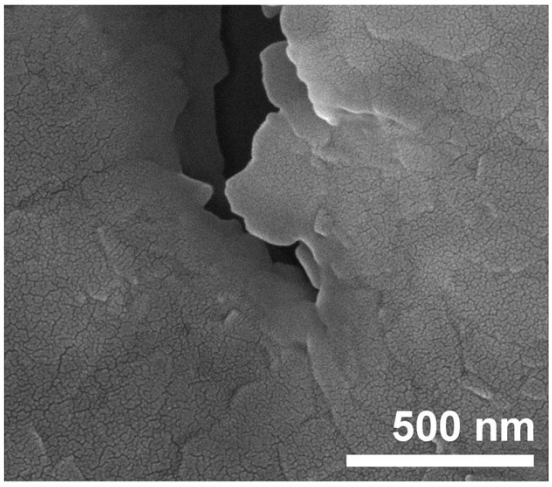

Fig. S11. The SEM image of N-PCNSs derived from ZIF-8 nanosheets.

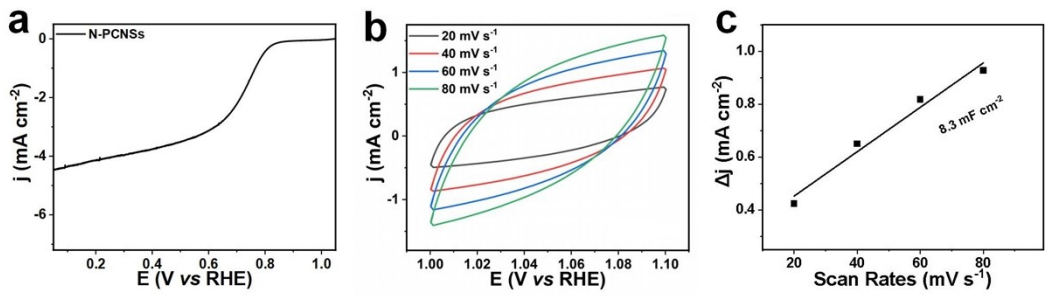

Fig. S12. (a) LSV curves of N-PCNSs. (b) CV curves at a potential range of 1.0 and 1.1 V at different scan rates and (c) corresponding electrochemical double layer capacitance values for N-PCNSs.

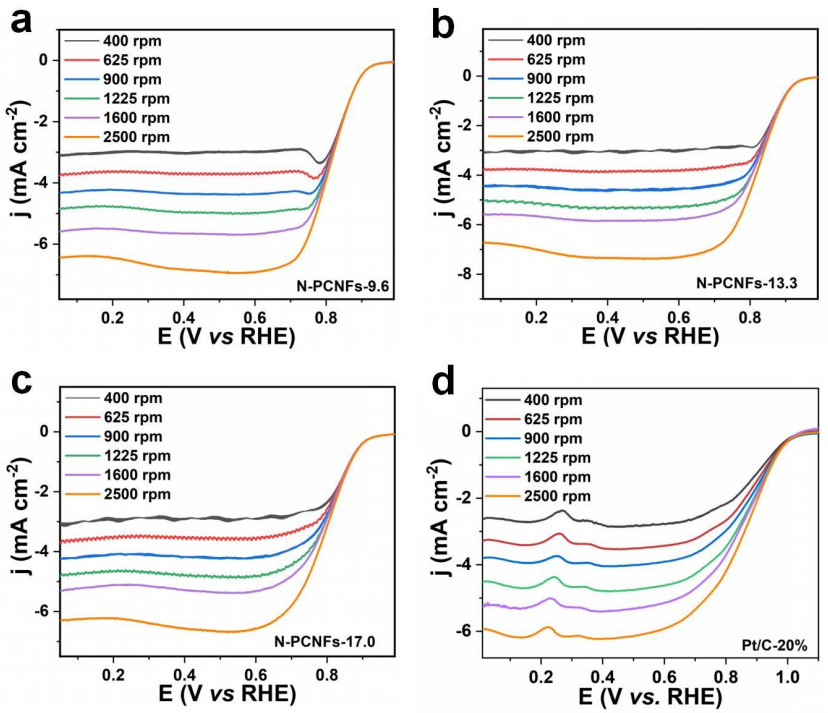

Fig. S13. LSV curves at various rotation speeds of (a) N-PCNFs-9.6, (b) N-PCNFs-13.3, (c) N-PCNFs-17.0 and (d) commercial Pt/C-20% catalyst.

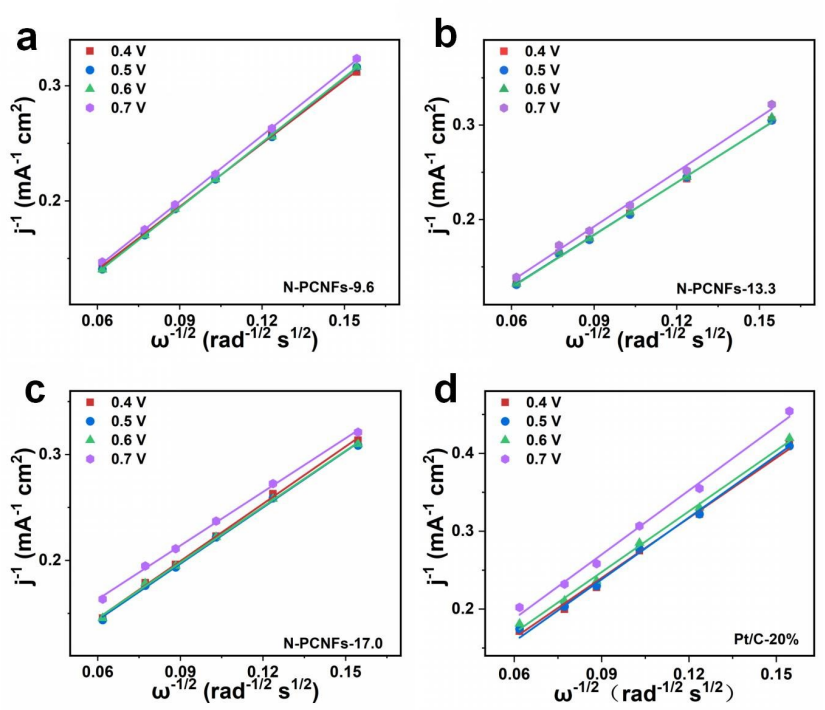

Fig. S14. K-L plots (j^{-1} *vs* $\omega^{-1/2}$) at different potentials of (a) N-PCNFs-9.6, (b) N-PCNFs-13.3, (c) N-PCNFs-17.0 and (d) commercial Pt/C-20% catalyst.

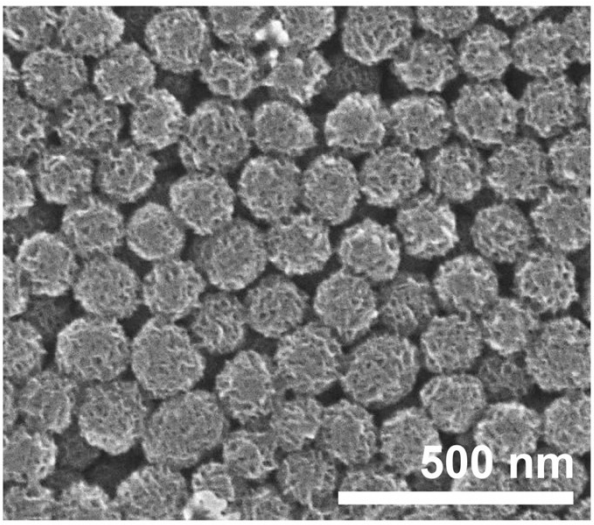

Fig. S15. The SEM image of N-PCNFs-43.5 after 10000 cyclic voltammetry cycles.

Table S1. The surface area, C_{dl} and ECSA of N-PCNFs.

Samples	BET surface area (m^2 g^{-1})	Micropore surface area (m^2 g^{-1})	External surface area (m^2 g^{-1})	C_{dl} (mF cm^{-2})	ECSA (m^2 g^{-1})
N-PCNFs-9.6	1956.0	1464.3	491.7	9.9	247.5
N-PCNFs-13.3	2109.6	1571.9	537.7	10.8	270.0
N-PCNFs-43.5	2018.6	1133.6	885.0	16.2	405.0
N-PCNFs-17.0	1552.3	1109.7	442.6	6.2	155.0

Table S2. Typical N species analysis of N-PCNFs samples.

Samples	Pyridinic-N (%)	Pyrrolic-N (%)	Graphitic-N (%)	Oxidized-N (%)
N-PCNFs-9.6	9.6	35.5	34.5	20.4
N-PCNFs-13.3	13.3	38.1	33.7	14.9
N-PCNFs-43.5	43.5	24.1	19.7	12.7
N-PCNFs-17.0	17.0	36.1	20.8	26.1

Table S3. Comparison of ORR performance with non-precious metal catalysts in 0.1 M KOH.

Samples	Half-wave (V *vs* RHE)	Onset potential (V *vs* RHE)	Decay after 10000 cycles (mV)	References
N-PCNFs-43.5	0.85	0.97	16	This work
FeNC	0.84	-	18	[S2]
Cu/SAC	0.81	0.97	-	[S3]
Cu-N/C	0.81	0.87	-	[S6]
Cu(15%)-MFC6	0.76	0.86	-	[S7]
Cu/Zn-NC	0.83	0.98	0	[S8]
CoNC700	0.80	0.96	0	[S9]
PPy/CuPcTs	0.78	0.92	-	[S10]
N-S/Gr-1000	0.79	0.92	20	[S11]
SA-Fe-HPC	0.81	0.94	-	[S12]
20Co-NC-1100	0.80	0.93	30	[S13]

References

[1] S1. W. Feng, M.M. Qin, P. Lv, J.P. Li and Y.Y. Feng, A three-dimensional nanostructure of graphite intercalated by carbon nanotubes with high cross-plane thermal conductivity and bending strength, *Carbon,* 2014, **77**, 1054-1064.

[2] S2. J.H. Roh, A. Cho, S.J. Kim, K.S. Lee, J. Shin, J.S. Choi, J. Bak, S.J. Lee, D.H. Song, E.J. Kim, C. Lee, Y.R. Uhm, Y.H. Cho, J.W. Han and E.A. Cho, Transformation of the active moiety in phosphorus-doped Fe-N-C for highly efficient oxygen reduction reaction, *ACS Catal.,* 2023, **13**, 9427-9441.

[3] S3. L.T. Cui, L.R. Cui, Z.J. Li, J. Zhang, H.N.Wang, S.F. Lu and Y. Xiang, A copper single-atom catalyst towards efficient and durable oxygen reduction for fuel cells, *J. Mater. Chem. A*, 2019, **7**, 16690-16695.

[4] S4. E. Zhu, C.Y. Shi, J. Yu, H.D. Jin, L.X. Zhou, X.K. Yang and M.L. Xu, Simultaneous regulation of thermodynamic and kinetic behavior on FeN_3P_1 single-atom configuration by Fe_2P for efficient bifunctional ORR/OER, *Appl. Catal. B-Environ.*, 2024, **347**, 123796-123809.

[5] S5. H. Li, G.L. Yan, H.Y. Zhao, P.C. Howlett, X.G. Wang and J. Fang, Earthworm-inspired $Co/Co_3O_4/CoF_2$@NSC nanofibrous electrocatalyst with confined channels for enhanced ORR/OER performance, *Adv. Mater.*, 2024, **36**, 2311272-2311288.

[6] S6. M.M. Fan, Q.X. Yuan, Y.Y. Zhao, Z.M. Wang, A. Wang, Y.Y. Liu, K. Sun, J.J. Wu, L. Wangh and J.C. Jiang, A facile “double-catalysts” approach to directionally fabricate pyridinic N-B-pair-doped crystal graphene nanoribbons/amorphous carbon hybrid electrocatalysts for efficient oxygen reduction reaction, *Adv. Mater.*, 2022, **34**, 2107040-2107051.

[7] S7. G. Saianand, A.I. Gopalan, J.C. Lee, C. Sathish, K. Gopalakrishnan, G.E. Unni, D. Shanbhag, V.D.B.C. Dasireddy, J. Yi, S. Xi, A.A.H. Al-Muhtaseb and A. Vinu, Mixed copper/copper-oxide anchored mesoporous fullerene nanohybrids as superior electrocatalysts toward oxygen reduction reaction,

Small, 2020, **16**, 1903937-1903948.

[8] S8. M.M. Tong, F.F. Sun, Y. Xie, Y. Wang, Y.Q. Yang, C.G.Tian, L. Wang and H.G. Fu, Operando cooperated catalytic mechanism of atomically dispersed Cu-N_4 and Zn-N_4 for promoting oxygen reduction reaction, *Angew. Chem. Int. Ed. Engl.*, 2021, **60**, 14005-14012.

[9] S9. J. Wang, Z. Huang, W. Liu, C. Chang, H. Tang, Z. Li, W. Chen, C. Jia, T. Yao, S. Wei, Y. Wu and Y.D. Li, Design of N-coordinated dual-metal sites: A stable and active Pt-free catalyst for acidic oxygen reduction reaction, *J. Am. Chem. Soc.*, 2017, **139**, 17281-17284.

[10] S10. Y. Meng, J. Yin, T. Jiao, J. Bai, L. Zhang, J. Su, S. Liu, Z. Bai, M. Cao and Q. Peng, Self-assembled copper/cobalt-containing polypyrrole hydrogels for highly efficient ORR electrocatalysts, *J. Mol. Liq.*, 2020, **298**, 112010-112018.

[11] S11. A. Arunchander, S.G. Peera, S.K. Panda, S. Chellammal and A.K. Sahu, Simultaneous co-doping of N and S by a facile in-situ polymerization of 6-N,N-dibutylamine-1,3,5-triazine-2,4-dithiol on graphene framework: An efficient and durable oxygen reduction catalyst in alkaline medium, *Carbon*, 2017, **118**, 531-544.

[12] S12. Z. Zhang, J. Sun, F. Wang and L. Dai, Efficient oxygen reduction reaction (ORR) catalysts based on single iron atoms dispersed on a hierarchically structured porous carbon framework, *Angew. Chem. Int. Ed. Engl.*, 2018, **57**, 9038-9043.

[13] S13. X.X. Wang, D.A. Cullen, Y.T. Pan, S. Hwang, M. Wang, Z. Feng, J. Wang, M.H. Engelhard, H. Zhang, Y. He, Y. Shao, D. Su, K.L. More, J.S. Spendelow and G. Wu, Nitrogen-coordinated single cobalt atom catalysts for oxygen reduction in proton exchange membrane fuel cells, *Adv. Mater.*, 2018, **30**, 1706758-1706767.